Title

Calculated cell-specific intracellular hydrogen peroxide concentration: Relevance in cancer cell susceptibility during ascorbate therapy

Authors

Erudaitius, Dieanira
Mantooth, Jacqueline
Huang, Andrew
et al.

Publication Date

2018-05-01

DOI

10.1016/j.freeradbiomed.2018.03.044

Calculated Cell-Specific Intracellular Hydrogen Peroxide Concentration: Relevance in Cancer Cell Susceptibility during Ascorbate Therapy

Dieanira Erudaitius[a], Jacqueline Mantooth[a], Andrew Huang[b], Jesse Soliman[a], Claire Doskey[c], Garry R. Buettner[d], Victor G. J. Rodgers[a,*]

[a]Department of Bioengineering, University of California, Riverside, Riverside, CA 92521, USA
[b]Department of Neuroscience, University of California, Riverside, Riverside, CA 92521, USA
[c]Center for Integrative Toxicology, Michigan State University, East Lansing, MI 48823, USA
[d]Free Radical & Radiation Biology, Department of Radiation Oncology, University of Iowa College of Medicine, Iowa City, IA 52242, USA.
*Corresponding Author, victor.rodgers@ucr.edu

FYI: Victor G. J. Rodgers ORCID is 0000-0002-1857-8025

Abstract

The high extracellular hydrogen peroxide (H_2O_2) concentrations generated during pharmacological ascorbate ($P\text{-}AscH^-$) therapy has been shown to exhibit a high flux into susceptible cancer cells leading to a decrease in clonogenic survival. It is hypothesized that the intracellular H_2O_2 concentration for susceptibility is independent of cell type and that the variation observed in dosing is associated with differences in the cell-specific overall steady-state intracellular H_2O_2 concentration values. The steady-state variation in intracellular H_2O_2 concentration is coupled to a number of cellular specific transport and reaction factors including catalase activity and membrane permeability. Here a lumped-parameter mathematical modeling approach, assuming a catalase-dominant peroxide removal mechanism, is used to calculate intracellular H_2O_2 concentration for several cell lines. Experimental measurements of critical parameters pertaining to the model are obtained. The cell lines investigated are normal pancreatic cells (H6c7), the pancreatic cancer cell line, MIA PaCa-2 and the glioblastoma cell lines, LN-229, T98G, and U-87; all which vary in susceptibility. The intracellular H_2O_2 concentration estimates are correlated with the clonogenic surviving fraction for each cell line, *in-vitro*. The results showed that, despite the fact that the experimental parameters including catalase concentration and plasma membrane permeability demonstrated significant variability across cell lines, the calculated steady-state intracellular to extracellular H_2O_2 concentration ratio did not vary significantly across cell lines. Thus, the calculated intracellular H_2O_2 concentration is not unique in characterizing susceptibility. These results imply that, although intracellular H_2O_2 concentration plays a key role in cellular susceptibility to $P\text{-}AscH^-$ adjuvant therapy, its overall contribution in a unifying mechanism across cell types is complex.

Keywords

Pharmacological ascorbate therapy; Hydrogen peroxide; plasma membrane permeability; peroxisome permeability; catalase; mathematical model; intracellular hydrogen peroxide concentration; cytosol; transport properties of cells; parameter sensitivity

Introduction

Pharmacological ascorbate ($P\text{-}AscH^-$) has demonstrated tremendous promise as an adjuvant in patients with pancreatic ductal adenocarcinoma [1, 2, 3, 4]. The current understanding of this phenomena is that $P\text{-}AscH^-$ serves as a pro-drug by its ability to generate high concentrations of extracellular hydrogen peroxide (H_2O_2) [4, 5, 6, 7, 8]. The extracellular H_2O_2 permeates the plasma membrane and, potentially, elevates the intracellular H_2O_2 concentration. Left unchecked, the high intracellular H_2O_2 reacts with labile iron that ultimately produces the highly reactive hydroxyl radicals [9]. The hydroxyl radical, in the vicinity of the nucleus, can generate cellular oxidative damage, especially to the DNA in cells and result in cytotoxicity [1, 2, 6, 10, 11, 12, 13,14, 15, 16, 17].

$P\text{-}AscH^-$ therapy has been found to have little effect on normal tissues. Once more, while $P\text{-}AscH^-$ therapy has been found to be successful for some pancreatic cancers, numerous *in-vivo* and *in-vitro* studies have demonstrated a range of susceptibility to $P\text{-}AscH^-$ therapy across various cancer cell types [1, 6,13, 14, 15, 16,18, 19, 20, 21, 22, 23]. The reason why some cancer cell lines are responsive to $P\text{-}AscH^-$ therapy while others are not remains elusive. However, at least two factors have been identified as to having a direct impact on the intracellular H_2O_2 concentration during $P\text{-}AscH^-$ therapy. These are; i) overall catalase activity and, ii) permeability of the plasma membrane to the flux of H_2O_2.

A family of intracellular enzymes exist to finely control the intracellular levels of H_2O_2, which normally exists around the 10 nM range [24]. Among them are the six peroxiredoxin enzymes, the glutathione peroxidase (GPx)/glutathione (GSH) system and catalase [27]. Catalase, in contrast to the other removal enzymes, is responsible for irreversibly consuming intracellular H_2O_2. At high concentrations H_2O_2, such as during pharmacological dosing associated with $P\text{-}AscH^-$ therapy, the rate of removal of peroxide is, essentially dominated by catalase [5,7,25,26,27,28]. Cohen and Hochstein showed that catalase became the dominant mechanism for removal of H_2O_2 in erythrocytes for concentrations greater than 1 μM [25]. Makino et al. (2004) found that the glutathione peroxidase (GPx)/glutathione (GSH) system was overwhelmed at about 50 μM of H_2O_2 and catalase became the dominant mechanism of peroxide removal for a number of mammalian cells [27]. Ng et al. (2007) estimated that the peroxide removal rate of the GPx/GSH system was reduced by three orders-of-magnitude when H_2O_2 concentrations were on the order of 5 μM for human glioma cells [28]. Thus, the assumption that the H_2O_2 removal rate is dominated by catalase at pharmacological peroxide dosing is a reasonable first-approximation.

Normal tissues have a relatively high catalase activity compared to cancer cells and it is believed that the intracellular H_2O_2 levels are below the toxicity range during $P\text{-}AscH^-$ therapy. The significance of catalase at high intracellular H_2O_2 concentrations justifies our focus on it as responsible for the primary intracellular reaction to remove the accumulating H_2O_2 during treatment.

Catalase activity vary widely across cell lines. Catalase activity is known to exhibit lower activity in tumor cells; where catalase expression ranges on the order of 10-100 fold times more for normal cells when compared to some tumor cells [29]. Other empirical studies have shown more than a 50% decrease in steady-state catalase activity for tumor cells [5]. This variation in catalase activity across cell lines could significantly affect the removal of H_2O_2, making tumor cells more susceptible to ascorbate mediated cell-death, as their capability to remove H_2O_2 is greatly hindered.

In addition to catalase activity, it has been recently shown that H_2O_2 permeability of the plasma membrane is a significant factor in cell susceptibility to extracellular H_2O_2 [30]. Peroxiporins (aquaporins that allow

transport of H_2O_2 across the plasma membranes), specifically AQP1, AQP3 and AQP8, are thought to be the principal pathways for the entry of H_2O_2 across the plasma membrane and that the flux of H_2O_2 across the plasma membrane is dominated by passive diffusion through these peroxiporins [31-33]. Many aquaporins are overexpressed in tumor cells of different origins, especially in aggressive tumors and it has recently been shown that pancreatic adenocarcinoma cells are believed to exhibit elevated AQP8 expression [33]. AQP3 has been found to increase by as much as eight-fold in cancer cells when treated with nucleoside analogs such as gemcitabine [34].

In our previous work, AQP3 was silenced in the MIA PaCa-2 pancreatic cancer cell line (siAQP3 MIA PaCa-2) and its clonogenic response was compared to unmodified MIA PaCa-2 for exposure to extracellular H_2O_2 concentrations equivalent to that generated during P-AscH$^-$ therapy dosing [30]. The results showed over twice the clonogenic surviving fraction for the siAQP3 MIA PaCa-2 when compared to MIA PaCa-2 for the highest dose. Thus, it is hypothesized the plasma membrane permeability differences, possibly due to the variability of peroxiporin expression across cell lines, can contribute to the variability of cell susceptibility to P-AscH$^-$ therapy. Figure 1 illustrates how the variations in catalase activity and peroxiporin expression might influence the cell susceptibility to ascorbate therapy.

Researchers have mathematically modeled the intracellular concentration of H_2O_2 primarily because of its critical significance in the homeostasis of the cellular redox environment [27,35,27,36]. The seminal work of Antunes and Cadenas (2000) provided a diffusion model based on latency of catalase to estimate intracellular H_2O_2 concentration. Ng et al. (2007) evaluated the range of H_2O_2 likely present during the GPx/GSH process during physiological conditions, but did not address the role of catalase [27]. Lim et al. (2015) developed a mathematical model for H_2O_2 in the cytosol under physiological conditions using a reduced kinetic model but did not consider catalase or membrane permeability [36].

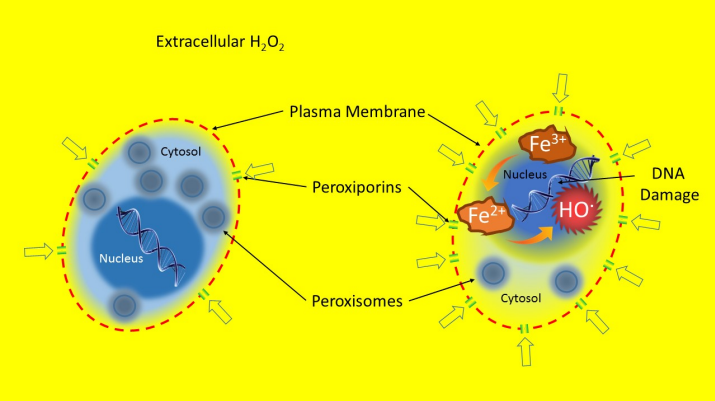

Figure 1. Illustration of the proposed dominant mechanisms for cellular susceptibility to ascorbate therapy. Ascorbate is introduced into the extracellular region by intravenous dosing that generates extracellular H_2O_2. The extracellular H_2O_2 enters the cell via its available peroxiporins at a rate consistent with the plasma membrane permeability and the effective catalase activity. In the figure to the left, it is proposed that normal cells and ascorbate-resistant cancer cells have either the ability to minimize peroxide permeability, rapidly catalyze intracellular hydrogen peroxide (via peroxisomes) and/or have limited labile iron present. The figure to the right illustrates susceptible cells which may have increased plasma membrane permeability to peroxide, reduced catalase activity and/or increased labile iron. The consequence of the chemical conditions in the susceptible cell is the generation of hydroxyl radicals near DNA that can result in damage and, ultimately, reduced clonogenic survival. This study focuses on quantifying the intracellular H_2O_2 concentration during P-AscH$^-$ therapy and determining its relationship and sensitivity to variations in catalase activity and plasma membrane permeability, both which have been found to vary across cell lines.

The overarching goal of this work is to elucidate why there is a variation in susceptibility to P-AscH$^-$ therapy dosing across cell lines when normalized to intracellular H_2O_2 concentration. Under this framework, the goal of this work is to provide a quantitative assessment of the intracellular H_2O_2 concentration associated with P-AscH$^-$

therapy for varying cell lines and determine if there is a correlation between the intracellular H_2O_2 concentration and the clonogenic response across cell lines. This work is the first to quantify intracellular H_2O_2 that is relevant to P-AscH$^-$ therapy. Further, this work examines the significant parameters associated with the intracellular H_2O_2 concentration and addresses whether their variability across cell lines is relevant. The critical issues addressed are; 1) the sensitivity of the intracellular H_2O_2 concentration to cellular variations in catalase activity and plasma membrane permeability, and, 2) the relationship between the intracellular H_2O_2 concentration, the previously observed cell line susceptibility to pharmacologic dosing of ascorbate and the clonogenic response of normal and cancer cell lines to the calculated intracellular H_2O_2 concentration. This work focuses on the pancreatic cell lines H6c7, MIA PaCa-2, siAQP3 MIA PaCa-2, and the glioblastoma cell lines, LN-229, T98G, and U-87. These glioblastoma cell lines have been found to range in susceptibility to ascorbate dosing *in-vitro* with LN-229 being highly susceptible, T98G being moderately susceptible and U-87 being insensitive [5].

This work begins with the development of the mathematical model used to estimate intracellular H_2O_2 concentration. In this development, measurable parameters associated with specific cell lines are identified and the expected sensitivity of these parameters on the intracellular H_2O_2 concentration are accessed. Next, experimental and modeling methods are combined to obtain the parameters needed to calculate the intracellular H_2O_2 concentration for the cells lines reviewed in this work. Finally, the intracellular H_2O_2 concentrations are calculated for each cell line and their sensitivity to significant parameters is analyzed. The calculated overall steady-state intracellular H_2O_2 to extracellular H_2O_2 ratio is plotted against previously reported ascorbate dosing results and the *in-vitro* surviving fraction from the clonogenic study for each cell line. These results are analyzed to determine whether intracellular H_2O_2 is the fundamental factor in dictating the cellular response to therapeutic levels of extracellular H_2O_2.

Mathematical methods

Governing equations

The generalized mathematical model for the conservation of mass of species *i* in a given closed mathematical volume, *V*, with surface area, *A*, can be expressed as

$$\frac{d}{dt}\int_V C_i dv = -\int_A \overrightarrow{n}\cdot\vec{N}_i\, da + \int_V R_i dv \tag{1}$$

where C_i is the molar concentration of species *i* in the volume, t is time, and $\frac{d}{dt}\int_V C_i dv$ is the rate of molar accumulation of species *i* in the prescribed volume. $\vec{N}_i$ is the flux of species *i* (moles of species *i* per area per time) and the integral $-\int_A \vec{n}\cdot\vec{N}_i\, da$ is the molar rate of species *i* entering into the volume across the surface area, *A*. The negative sign accounts for the direction of the outward bound normal $\vec{n}$ that is used to define the orientation of the surface. R_i is the net molar rate of formation of species *i* per volume so $\int_V R_i dV$ is the rate of the moles of species *i* that is generated in the volume due to its production. Because this model is the integral of the concentration in differential volumes (dv), it captures the variation in the concentration of species *i* in both time and space. Nevertheless, this form of the conservation of mass is advantageous as it provides the foundation for the assumptions of the idealized model used in this work.

In particular, the idealized model assumes that the concentrations in all of the volumes in question are relatively independent of spatial variations and, thus, the conservation of species *i* is a function of only

time (lumped parameter model or well-mixed assumption). Under this assumption, Eqn 1 can be integrated to the entire volume and becomes

$$V\frac{dC_i}{dt} = N_i|_A A + R_i V. \tag{2}$$

Here we expressed the molar flux of species *i* in its scalar form, $N_i|_A$, and allow A to represent the area of the volume in which species *i* enters the volume.

For the analysis of intracellular H_2O_2 concentration (in the cytosol) during ascorbate therapy, we consider three volumes, the volume of the extracellular compartment, V_{ext}, the volume of the cytosol, V_{in}, and the volume of the peroxisomes, V_p, where cytosolic H_2O_2 permeates and is converted via catalase. Thus, three equations are necessary to capture the overall mass balance of H_2O_2 in this system. Figure 2 illustrates the selected system used in this analysis. The corresponding concentrations of H_2O_2 in the extracellular region, the cytosol and in the peroxisomes are, C_{ext}, C_{in}, and C_p, respectively.

The transport mechanism of H_2O_2 across the plasma membrane and peroxiporins is passive diffusion and, thus, the driving force is the concentration gradient at the interface area between volumes. To eliminate spatial dependency, the flux is represented by the concentration differences in each volume at the interface and a membrane permeability. Assuming a dilute solution, the Fickian model for N_i can be described as

$$N_i|_A = -D_{ij}\nabla C_i|_{interface} \approx m_k\left(C_{i,V_{k+1}} - \varphi_k C_{i,V_k}\right) \tag{3}$$

where D_{ij} is the Fickian diffusion coefficient of species *i* in solvent *j*, $\nabla C_i|_{interface}$ is the concentration gradient at the interface of the adjacent volumes (for one-dimensional radial direction $\nabla C_i|_{interface} = \frac{\partial C_i}{\partial r}\Big|_{r=R}$), m_k is the membrane permeability associated with the area interface for the k^{th} volume, V_k, and V_{k+1} in the adjacent volume at the transport interface. The partition coefficient, φ_k, is used to correct for thermodynamic equilibrium for concentrations across interfaces. Note that the membrane permeability

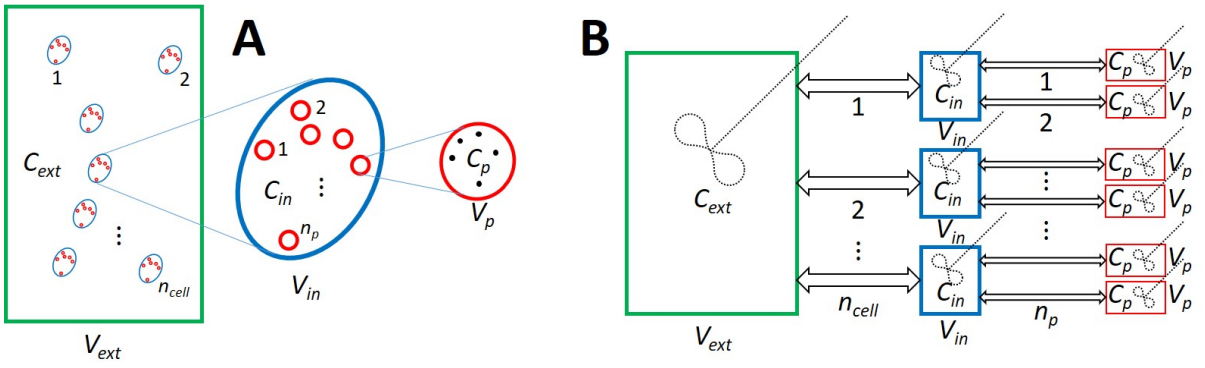

Figure 2. Illustration of the proposed modeling approach for the fate of extracellular H_2O_2 permeating into cells. In Fig 2A, the external H_2O_2 concentration (C_{ext}) permeates into each of the n_{cell} cells via diffusion. The resulting intercellular H_2O_2 (concentration C_{in}) can, subsequently, diffuse across the peroxisome membranes into the n_p peroxisomes per cell where it is converted by catalase. The concentration of H_2O_2 in the peroxisomes is denoted by C_p. The volumes for the chambers are V_{ext}, V_{in}, and V_p, for the extracellular, intracellular (cytosolic) and the peroxisomes, respectively. Fig 2B is the idealized lump parameter model for the system. Here concentration is assumed to be spatially independent in all compartments (illustrated by the well-mixed impeller symbol). The flux of H_2O_2 across chambers is denoted by the double arrows. In this modeling effort, the flux is modeled using membrane permeability with concentration difference across chambers as the driving force.

represents the diffusivity of the species divided by a characteristic length of the system. The approximation on the right-hand side of Eqn (3) uses the concentration difference across the interface which is indicative for passive diffusion and is equivalent to the numerical approximation for diffusive flux. The current model allows flux to reduce and establish equilibrium with non-zero species *i* concentrations. Letting species *i* be H_2O_2, Eqns. (2) and (3) can be combined to provide the idealized lumped parameter for H_2O_2 in this study.

Assuming a dilute concentration of H_2O_2, Eqns (1-3) is used for all compartments to obtain,

$$V_{ext}\frac{dC_{ext}}{dt} = M_{in}\delta(t) - m_{plm}A_{cell}n_{cell}\left(\varphi_{plm}C_{ext} - C_{in}\right) \quad (4)$$

$$V_{in}\frac{dC_{in}}{dt} = m_{plm}A_{cell}\left(\varphi_{plm}C_{ext} - C_{in}\right) - m_pA_pn_p\left(\varphi_pC_{in} - C_p\right) \quad (5)$$

$$V_p\frac{dC_p}{dt} = m_pA_p\left(\varphi_pC_{in} - C_p\right) - k_2C_{cat_p}C_pV_p. \quad (6)$$

Here, m_{plm} and m_p, represent the plasma membrane permeability and the peroxisome membrane permeability, respectively. The parameters φ_{plm} and φ_p are the partition coefficients of the plasma membrane and peroxisome membrane, respectively. For this study, these values are assumed to be unity. The initial moles of H_2O_2 added in the extracellular compartment is denoted as M_{in}, A_{cell} is the area of a cell, n_{cell} is the number of cells in V_{ext}, and $\delta(t)$ is the Dirac delta function with units of inverse time. No reaction is assumed to take place in the extracellular or cytosolic volume. The catalase reaction of H_2O_2 is assumed to occur within the peroxisomes, and, here, $R_i = -k_2C_{cat_p}C_p$. Here k_2 is the effective second order reaction rate of H_2O_2 decomposition by catalase, and we define C_{cat_p} as the concentration of catalase inside each peroxisome [37].

Steady-state model for intracellular H2O2 concentration

The steady-state intracellular H_2O_2 concentration that corresponds to the extracellular H_2O_2 concentration can be obtained by setting the time derivatives of Eqn (5) and (6) to zero while assuming C_{ext} is constant. The resulting dimensionless intracellular H_2O_2 concentration is

$$\theta_{ss} = \frac{C_{in}}{\varphi_{plm}C_{ext}} = \frac{m_{plm}A_{cell}\varphi_{plm}\left(m_pA_p + k_2C_{cat_p}V_p\right)}{m_{plm}A_{cell}\left(m_pA_p + k_2C_{cat_p}V_p\right) + m_pA_pn_p\varphi_pk_2C_{cat_p}V_p}. \quad (7)$$

From a practical perspective, the concentration of catalase extracted per cell, $C_{cat_{cell}}$ can be used giving

$$\theta_{ss} = \frac{m_{plm}A_{cell}\varphi_{plm}\left(m_pA_p + k_2\frac{C_{cat_{cell}}V_{cell}}{n_p}\right)}{m_{plm}A_{cell}\left(m_pA_p + k_2\frac{C_{cat_{cell}}V_{cell}}{n_p}\right) + m_pA_pn_p\varphi_pk_2\frac{C_{cat_{cell}}V_{cell}}{n_p}}. \quad (8)$$

It is instructive to note that the above models satisfy the asymptotic limits for $\frac{C_{in}}{C_{ext}}$. Assuming a partitioning coefficient of 1, ($\varphi_{plm} = 1$), if no catalase activity, then $k_2C_{cat_p} \to 0$ and the solution to Eqn (7) approaches unity. In addition, at high catalase where $k_2C_{cat_p} \gg \frac{m_pA_p}{V_p}$, then $\theta_{ss} \to 0$. This model provides a convenient format for addressing the dependency of the steady-state intracellular H_2O_2 concentration on various parameters as well as provides a convenient format for sensitivity analysis.

Sensitivity of intracellular H2O2 concentration to catalase activity and plasma membrane permeability

Catalase activity and plasma membrane permeability have been identified as two parameters that vary across cell lines and could, subsequently, impact the intracellular H_2O_2 concentration during ascorbate therapy. Local sensitivity analysis is used to estimate the impact of these parameters on θ_{ss}. Using the dimensionless sensitivity parameter, $s_{\theta,j}$, defined as the local derivative of θ_{ss} with respect to the j^{th} normalized parameter [38], we obtain the following sensitivity parameter for the plasma membrane permeability and catalase activity,

$$s_{\theta,m_{plm}} = \frac{A_{cell}k_2Cat_pm_pn_pA_p\varphi_p\varphi_{plm}V_p\left(m_pA_p+k_2C_{cat_p}V_p\right)m_{plm}}{\left[m_{plm}A_{cell}\left(m_pA_p+k_2C_{cat_p}V_p\right)+k_2C_{cat_p}V_pm_pn_pA_p\varphi_p\right]^2}, \quad (9)$$

$$s_{\theta,C_{cat_p}} = \frac{-m_{plm}A_{cell}(m_p)^2n_p(A_p)^2k_2\varphi_p\varphi_{plm}V_pC_{cat_p}}{\left[m_{plm}A_{cell}\left(m_pA_p+k_2C_{cat_p}V_p\right)+k_2C_{cat_p}V_pm_pn_pA_p\varphi_p\right]^2}, \quad (10)$$

and

$$s_{\theta,m_p} = \frac{-m_{plm}\left(C_{cat_p}\right)^2A_{cell}(k_2)^2n_pA_p\varphi_p(V_p)^2\varphi_{plm}m_p}{\left[m_{plm}A_{cell}\left(m_pA_p+k_2C_{cat_p}V_p\right)+k_2C_{cat_p}V_pm_pn_pA_p\varphi_p\right]^2}. \quad (11)$$

Localized sensitivity analysis expressions for other parameters are listed in Supplemental I.

Validity of the lumped parameter model

Significance of spatial dependency in the cytosol

Eqn (7) provides a simple approach to estimating the intracellular H_2O_2 concentration during high dosing of extracellular peroxide. However, this method has several limitations that must be addressed when determining the validity of the solution. To begin, the lumped parameter model assumes the H_2O_2 concentrations are spatially independent. To check the validity of this approximation for the cytosol, we begin by looking at the potential for concentration gradients to exist by modeling this volume using a steady-state diffusion problem with a pseudo-homogeneous reaction. The pseudo-homogenous reaction model assumes that the peroxisomes are well distributed and the catalase-related reaction is carried out throughout the volume. For this approach, the cell is assumed to be spherical with a radius of r_c and the nucleus with a radius of r_n. Figure 3 illustrates the geometry for this model. The dashed enclosed lines in Fig 3 in the intracellular volume illustrates the control volume concept under consideration. In this approach, the control volume is sufficiently large to contain the peroxisomes but assumed to be small enough to apply the continuum model for the conservation of mass. Using Eqn (1) and converting the area integral to a volume integral and assuming spherical coordinates we obtain,

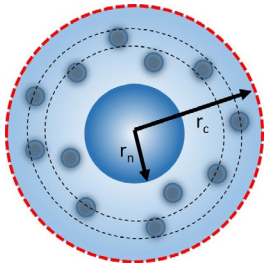

Figure 3. Illustration of the model used to examine the spatially dependent intracellular H_2O_2 concentration in the cytosol. In this model, it is assumed that the peroxisomes are well dispersed in the cytosol and result in a pseudo-homogeneous reaction approximation. The area between the inner dashed lines represent the control volume used in Eqn (12).

$$\frac{\partial C_{in}}{\partial t} = D_{ij}\frac{1}{r^2}\frac{\partial}{\partial r}\left(r^2\frac{\partial C_{in}}{\partial r}\right) + R_i \quad (12)$$

The peroxisomes are present in the region $r_c \geq r > r_n$ and $R_i = -k_2^* \rho_p C_{in}$ where ρ_p is the number density of peroxisomes in the volume, and k_2^* is the effective second-order reaction rate constant for the observed reaction. The parameter k_2^* is specific to each cell line and absorbs variations in latency, and catalase activity.

Assuming steady-state, Eqn (12) becomes

$$D_{ij} \frac{1}{r^2} \frac{d}{dr}\left(r^2 \frac{dC_{in}}{dr}\right) = -R_i. \tag{13}$$

In determining an appropriate set of boundary conditions, it is assumed that in the nucleus ($r_n \geq r \geq 0$), $R_i = 0$. Thus, at the nucleus wall, the flux of H_2O_2 is zero. At the plasma membrane wall, the diffusive flux into the cell is equivalent to the mass flux across the membrane into the cell. Thus, the boundary conditions can be written as

$$dC_{in}(r_n)/dr = 0$$

and

$$-\varphi_{plm} D_{ij} dC_{in}/dr|_{r=r_c} = m_{plm}\left(\varphi_{plm} C_{ext} - C_{in}|_{r=r_c}\right). \tag{14}$$

The dimensionless form of this problem can provide tremendous insight as it allows one to compare appropriate dimensionless groups across cell lines. Defining a dimensionless concentration, $\theta_\eta \equiv C_{in}(r)/\varphi_{plm} C_{ext}$, dimensionless radius, $\eta \equiv r/r_c$, the Thiele modulus for the cell, $\phi_c \equiv \sqrt{k_2^* \rho_p r_c^2 / D_{ij}}$, and the characteristic time, $t^* \equiv \frac{r_c^2}{D_{ij}}$, Eqn (12) can be written as

$$\frac{\partial \theta_\eta}{\partial t} = \frac{1}{\eta^2} \frac{\partial}{\partial \eta}\left(\eta^2 \frac{\partial \theta_\eta}{\partial \eta}\right) - {\phi_c}^2 \theta_\eta. \tag{15}$$

When C_{ext} is constant, the system is assumed to reach steady-state when $t \gg t^*$. Assuming the diffusion coefficient for H_2O_2 in water is 1.4 x 10^{-9} m s^{-1} [39], for a typical cell radius of 10 μm, t^*= 7 x 10^{-2} s. All studies in this work satisfy this condition so Eqn (15) reduces to

$$\frac{1}{\eta^2} \frac{d}{d\eta}\left(\eta^2 \frac{d\theta_\eta}{d\eta}\right) = {\phi_c}^2 \theta_\eta. \tag{16}$$

Defining $\lambda \equiv r_n/r_c$, the boundary conditions become

$$d\theta_\eta(\lambda)/d\eta = 0$$

$$-d\theta_\eta/d\eta\big|_{\eta=1} = Bi_c\left(1 - \theta_\eta(1)\right). \tag{17}$$

where $Bi_c \equiv m_{plm} r_c/(\varphi_{plm} D_{ij})$ is the Biot number for the cell.

The generalized solution of Eqn (16) for arbitrary λ subject to the boundary conditions (Eqn (17)) can be found in Supplemental II. When is $\lambda = 0$, the solution becomes

$$\theta_\eta = \frac{Bi_c \sinh(\phi_c \eta)}{\eta[\phi_c \cosh(\phi_c) + (Bi_c - 1)\sinh(\phi_c)]}. \tag{18}$$

This conservative solution where $\lambda = 0$ is sufficient for determining whether spatial dependency is significant in the cytosol. Assigning $\eta = 0$ to Eqn (18) and applying L'Hospital's Rule, the assumption of spatial independence is valid provided,

$$\theta_{\eta=0}/\theta_{\eta=1} = \frac{\phi_c}{sinh(\phi_c)} \approx 1. \quad (19)$$

Pseudo steady-state assumption

The assumption that C_{ext} is constant is valid for an infinite source approximation (relatively large volume). For studies that require a finite V_{ext} however, this approximation is reasonable provided the time for the steady is substantially less than the process overall time constant. A conservative overall time constant can be determined by reviewing Eqn (4) and assuming $C_{in} \approx 0$. Then the process overall time constant, $t_{overall}$, can be written as

$$t_{overall} \equiv \frac{V_{ext}}{\varphi_{plm} m_{plm} A_{cell} n_{cell}}. \quad (20)$$

Thus, the steady-state approximation provides a reasonable approximation when the final time for the study, t_f is such that $t_f \ll t_{overall}$.

Estimation of average external H_2O_2 for clonogenic assay

When t_f is on the order of $t_{overall}$ or greater, the external concentration in the sample volume can reduce with time. For a matter of dosing, the timed-average external concentration, $\bar{C}_{ext}$, can be used to represent the dosing concentration during the study. This value can be determined by solving for $C_{ext}(t)$ using Eqn (4 – 6) and numerically determining

$$\bar{C}_{ext} = \frac{1}{t_f} \int_0^{t_f} C_{ext}(t) dt. \quad (21)$$

Experimental methods and approach

The primary objective is to compare the calculated dimensionless steady-state intracellular H_2O_2 concentration, θ_{ss}, for various extracellular H_2O_2 dosing concentration for each cell line to the clonogenic response. The clonogenic response is based on the surviving fraction and is calculated for each cell line for extracellular H_2O_2 dosing. In addition, parameter values and sensitivity of θ_{ss} are determined. As the parameters for each cell line are not available in the literature, each related parameter is experimentally measured.

Parameters required to calculate θ_{ss}

Equations (7) and (8) show that θ_{ss} is a function of, not only the plasma membrane and peroxisome membrane permeabilities and catalase concentration, but also the geometric properties of the cell and peroxisome number density. The sensitivity analysis associated with the membrane permeabilities and catalase concentration are also function of other variables, requiring error propagation for completeness.

Imaging and spectroscopy methods and mathematical analysis of results from H_2O_2 uptake studies are used to determine each parameter. From Eqns (7) and (8), the parameters that are determined are: cell and peroxisome average areas, A_{cell} and A_p, respectively, the peroxisome volume, V_p, volume of the cell, V_{cell}, number of peroxisomes, n_p, the catalase concentration per cell, $C_{cat_{cell}}$ and the plasma membrane and peroxisome membrane permeabilities, $m_{plm}$and m_p, respectively.

The resulting values for each parameter are used to calculate θ_{ss} for each cell line using Eqn (8). Error for θ_{ss} is determined by propagation of error for each measured parameter.

Materials and preparation methods

Cells and reagents

Pancreatic H6c7 cells (HPV16-E6E7) [40] are established by transduction of HPV16-E6E7 genes into a primary culture of normal pancreatic duct epithelial cells and cultured in keratinocyte SFM (KSFM, Invitrogen, Carlsbad, CA) with supplements: human recombinant epidermal growth factor and bovine pituitary extract (Life Technologies, Carlsbad, CA, USA). Pancreatic adenocarcinoma MIA PaCa-2 cells (American Type Culture Collection Manassas, VA, USA) are cultured in Dulbecco's Modified Eagle's Medium (DMEM, American Type Culture Collection Manassas, VA, USA) with 10% fetal bovine serum (FBS, ThermoFisher Scientific, Lafayette, CO, USA). Glioblastoma U-87 MG cells (American Type Culture Collection Manassas, VA, USA) are cultured in Eagle's Minimum Essential Medium (EMEM, American Type Culture Collection Manassas, VA, USA) with 10% fetal bovine serum (FBS, ThermoFisher Scientific, Lafayette, CO, USA). Glioblastoma T98G cells (American Type Culture Collection Manassas, VA) are cultured in Eagle's Minimum Essential Medium (EMEM American Type Culture Collection Manassas, VA, USA) with 10% fetal bovine serum (FBS, ThermoFisher Scientific, Lafayette, CO, USA). Glioblastoma LN-229 (American Type Culture Collection Manassas, VA, USA) are cultured in Dulbecco's Modified Eagle's Medium (DMEM, American Type Culture Collection Manassas, VA, USA) with 5% fetal bovine serum (FBS, ThermoFisher Scientific, Lafayette, CO, USA). All cells are maintained at incubation of 37°C and supplied with 5% CO_2 and 1% penicillin streptomycin (Life Technologies, Carlsbad, CA, USA).

Peroxisome isolation

Peroxisomes are extracted from cells using a fractionation centrifugation method. The series of centrifugations are adjusted from the protocol provided by Sigma-Aldrich (Peroxisome Isolation kit, PEROX1, Sigma-Aldrich, St. Louis, MO, USA). Cells are seeded into HyperFlask M cell culture vessels (13700420, Corning, Union City, CA, USA) and incubated at 37 °C until 100% confluency is reached (2 x 10^8 cells). Cells are harvested using accutase (25-058-CI, Sigma-Aldrich, St. Louis, MO, USA)(50 mL) and PBS (50 mL) is added to increase the volume to extract all cells from the HyperFlask. Accutase is quenched using FBS (100 mL) and the cell suspension (200 mL) is transferred and, subsequently, centrifuged (Marathon 8K Centrifuge, Beckman Coulter, Brea, CA, USA) 3x at 2,364 rpm (250 x g) for 5 min at room temperature. The supernatant is discarded and cells are re-suspended in 15 mL PBS between spins. Before the final spin, the number of cells are determined using a Moxi Z Mini Automated Cell Counter. A packed cell volume (PCV) (1 – 3 mL), resulting from the third spin, is re-suspended in ice-cold (4°C) 1x peroxisome extraction buffer (PEB) (4 – 5 mL) (7247, Sigma-Aldrich, St. Louis, MO, USA) containing protease inhibitor cocktail 1% (v/v)(P8340, Sigma-Aldrich, St. Louis, MO, USA). The suspension is transferred to a 7 ml Dounce glass tissue grinder (T0566, Sigma-Aldrich, St. Louis, MO, USA) and a clearance pestle (P1235, Sigma-Aldrich, St. Louis, MO, USA) is used to cause 80 – 85% breakage (~7 strokes). Cell aliquots are stained using Trypan Blue (Sigma-Aldrich, St. Louis, MO, USA) every 5 strokes and counted (dilution factor of 5) using a hemocytometer to monitor breakage. After sufficient cell breakage, cells are centrifuged (Optima ultracentrifuge, Beckman Coulter, Brea, CA, USA) at 3,400 rpm (500 x g) (Type 90 Ti rotor) for 10 min at 4°C. The supernatant is transferred to ice while the pellet is re-suspended in 1x PEB (4 – 5 ml) and subsequently centrifuged at 3,400 rpm (500 x g) for 10 min at 4°C. The supernatants are combined in a new tube and spun at 8,400 rpm (6,000 x g) for 10 min at 4°C. The supernatant is transferred to a new tube and centrifuged at 15,000 rpm (20,000 x g) for 15 min at 4°C. The supernatant is discarded and the pellet re-suspended in ice cold (4°C) 1x PEB. Cells are centrifuged at 4,200 rpm (1500 x g) for 10 min at 4°C to result in a crude peroxisome fraction (CPF). The CPF (1.2 mL) is diluted in the Optiprep density gradient (1.69 mL) (D1556, Sigma-Aldrich, St. Louis, MO, USA) and 1x

Optiprep dilution buffer (1.61 mL) (O4889, Sigma-Aldrich, St. Louis, MO, USA). The CPF (4 mL) is then layered between a 27.5% (2 mL) and 20% (2 mL) Optiprep density gradient (D1556, Sigma-Aldrich, St. Louis, MO, USA). The sample is centrifuged at 34,163 rpm (100,000 x g) for 1.5 h at 4°C. Samples following the final centrifugation, if stored, remain in the 4°C for a maximum of 24 h before studies are conducted.

Determining number of peroxisomes, n_p, peroxisome area, A_p, and peroxisome volume, V_p

Cells are seeded on glass cover slips (ThermoFisher Scientific, Lafayette, CO, USA) in complete growth medium and incubated at 37 °C, 5 % CO_2 for 48 h to allow 70% confluency to be reached. Adhered cells are transduced with 50 particles per cell (PPC) of CellLight Regents BacMam 2.0 (C10604, ThermoFisher Scientific, Lafayette, CO, USA) and mixed gently to allow peroxisome tagging. GFP transduced cells are incubated at 37 °C, 5 % CO_2 for 48 h before fixing with paraformaldehyde (4% PFA) for 15 min. PFA is removed by three 5-min 1x PBS washes. Glass coverslips containing GFP-tagged peroxisome cells are mounted on microscope slides (ThermoFisher Scientific, Lafayette, CO, USA).

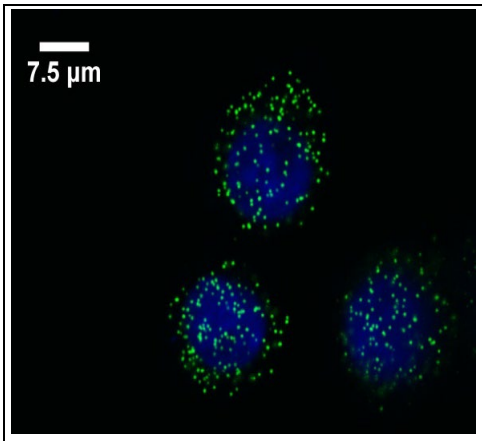

Figure 4. An example image of normal pancreatic (H6c7) cells taken from a series of z-stack images using the Leica SP5 confocal microscope to identify peroxisomes per cell. The image displays the nucleus (blue) and peroxisomes (green). Peroxisomes were counted in each z-stack slice to obtain the number of peroxisomes per cell.

Z-stack images are taken with the Lecia SP5 confocal microscope (Lecia, Solms, Germany) and analyzed using ImageJ (NIH). Z-stack images are taken to visualize the entire cell and peroxisomes are counted per slice for each cell line to obtain the number of peroxisomes per cell, n_p. Figure 4 illustrates an example of the Z-stack images used.

ImageJ (NIH) is used to measure the radius for each peroxisome in triplicate. Assuming spherical geometry, the radial measurements are used to determine the average peroxisome area, A_p, and volume, V_p.

Determining area of the cell, A_{cell}

To determine the cell area, A_{cell}, the cell-specific radius is obtained using an automated cell counter (Moxi Z Mini Automated Cell Counter, ORFLO Technologies, Ketchum, ID, USA). Assuming a spherical cell, A_{cell} is calculated for each cell type.

Determining cytosol volume, V_{cell}

The cell volume, V_{cell}, is associated with the volume of the cell occupied by the peroxisomes. Thus V_{cell} is determined by substracting the nucleus volume from the estimated total cell volume determined from the cell-specific radius provided by the automated cell counter (Section 3.4). The nucleus volume is obtained by first using NucBlue Live Cell Stain ReadyProbes reagent (R37605; Life Technologies, Carlsbad, CA, USA) to stain the nucleus of the cells during the imaging process outlined in Section 3.3. ImageJ (NIH) is used to calculate the elliptical area for each z-stack obtained during the confocal imaging process. The nucleus volume is calculated by multiplying each elliptical area by the z-stack thickness and summing all elliptical sections for each nucleus examined on each plane. The cell volume, V_{cell}, is determined by subtracting the calculated nucleus volume from the estimated total cell volume.

Determination of catalase concentration, C_{cat_p} and $C_{cat_{cell}}$

Catalase concentration, C_{cat_p}, is measured in each cell lysate using a spectrophotometric-based assay [41]. Cells are harvested at a density of (1.0 – 5.0) x 10^6 cells in PBS (3 mL) using a cell scraper (Fisher Scientific, Pittsburgh, PA, USA). The cell count is determined using a MoxiZ Mini Automated Cell Counter to provide the number of cells used in the assay. Scraped cells are centrifuged (Marathon 8K Centrifuge) at 1000 rpm for 5 min. Cells are re-suspended in PBS (1 mL) and transferred to an Eppendorf tube (Fisher Scientific, Pittsburgh, PA, USA) and subsequently centrifuged (Marathon 8K Centrifuge) 2x at 1000 rpm for 5 min. Following the last spin, PBS (1 mL) is layered on top of the pellet and placed in the freezer (-80 °C) for 24 h. Cells are then sonicated (Qsonica, Newtown, CT, USA) 4x for 10 sec intervals with 30 s breaks at 100% amplitude to fully lyse the cells. It is assumed that the catalase is fully released from sonication and is well dispersed into the suspension of the lysate. The cell lysate is further diluted in 50 mM phosphate buffer (pH 7.0), placed in a quartz cuvette (Thorlabs, Newton, NJ, USA) and, 30 mM H_2O_2 (Sigma-Aldrich, St. Louis, MO, USA) is added. The H_2O_2 consumption is followed by the decay in absorbance (@240 nm) over time. Absorbance is measured every 10 s for a total of 25 min. The slope of the logarithmic curve (ln[H_2O_2 absorbance] vs. time (s)) provides the observed rate (k_{obs}) of H_2O_2 consumption. Using the catalytic rate constant per monomer [37], $k_2 = 1.7\ x\ 10^7\ M^{-1}\ s^{-1}$, and the known number of cells in the chamber (n_{cell}), k_{obs} is used to calculate the active catalase molecules per cell. Acknowledging catalase as a tetramer, the number of tetramers per cell is ¼ the monomer count. Subsequently, the confocal images provide the number and volume of peroxisomes for each cell and, thus, allows $C_{cat_p} = \left[\frac{Cat_{cell}}{V_p\ n_p}\right]$ to be determined. The error in $C_{cat_p}$is determined by propagating the error associated with $C_{cat_{cell}}$, the number of peroxisomes per cell, n_p, and the volume of the peroxisome V_p.

Determining peroxisome membrane permeability, m_p

The rate of H_2O_2 uptake for intact peroxisomes extracted from all cells are measured in a similar fluorescent based manner as described previously by Wagner et al. [43]. The adjusted protocol measures the change in extracellular H_2O_2 over time, which decays exponentially representing a pseudo-first order behavior of the intracellular catalase reaction. The technique is a highly sensitive fluorescent method capable of detecting low concentrations of H_2O_2, below 0.5 µM. Isolated peroxisomes (specific to each case) are diluted in 50 mM phosphate buffer (pH 7.0) and placed into a reaction chamber (6 mL). The reaction chamber (roughly $(7 - 12)\ x\ 10^8$ peroxisomes) is initiated by the addition of an extracellular bolus of 30 mM H_2O_2 (Sigma-Aldrich, St. Louis, MO, USA) and aliquots (30 µL, chosen to prevent >10% of total volume from being removed) are taken at specified time points (0, 2, 8, 10, 12, 14, 16, 18, 20, and 25 min). Aliquots are transferred in duplicate to designated $2\ x\ 10^2$ µL wells of 96-well culture (Corning, Union City, CA, USA) dish. The wells (F2-F11, G2-G11) contain phosphate buffer (30 µL) and a quenching solution (60 µL) comprised of 20 mL phosphate buffer (pH 7.0), 20 µL 1M 4(–2–hydroxyethyl)–1–piperazineethansulfonic acid (HEPES) (pH 7.2 – 7.5) (ThermoFisher Scientific, Lafayette, CO, USA), 10 mg $NaHCO_3$ (3mM) (ThermoFisher Scientific, Lafayette, CO, USA), 5 mg 4-hydroxyphenylacetic acid (*p*HPA) (Sigma-Aldrich, St. Louis, MO, USA), and 2 mg HRP (horse radish peroxidase Type 1) (Sigma-Aldrich, St. Louis, MO, USA). The stopping solution is used to terminate peroxisome uptake at the desired time point. The quenching solution prevents any remaining H_2O_2 from entering the peroxisome as H_2O_2 instead activates HRP which in turn oxidizes *p*HPA resulting in the fluorescent *p*HPA dimer. The fluorescent signal is representative of the H_2O_2 concentration in each well and is further detected via the Tecan F200 (Tecan US, Morrisville, NC) plate reader with an excitation at 340 nm (bandwidth 20 nm) and monitoring an

emission at 430 nm (bandwidth 20 nm) from above the wells. Additionally, designated wells (B2 – B11, C2 – C11, D2 – D11) contain standard solutions (60 µL) having ten different final concentrations of H_2O_2 (4, 3.6, 3.2, 2.8, 2.4, 2, 1.6, 1.2, 0.8, 0.4 mM) after the addition of the stopping solution (60 µL), completing a final volume of 120 µL. The number of peroxisomes in the reaction chamber are determined after knowing the peroxisome count per cell (see Section 3.3) and determining the number of cells using a Moxi Z Mini Automated Cell Counter used during the peroxisome extraction.

The transient data for C_{ext} is used to determine the value of the peroxisome membrane permeability (m_p) by regression using the model,

$$V_{ext}\frac{dC_{ext}}{dt} = M_{in}\delta(t) - m_p A_p n_p\left(\varphi_p C_{ext} - C_p\right) \tag{22}$$

$$V_p\frac{dC_p}{dt} = m_p A_p\left(\varphi_p C_{ext} - C_p\right) - k_2 C_{cat_p} C_p V_p, \tag{23}$$

where V_{ext} is now the total volume of extracellular media. Following an appropriate initial guess, a Levenberg-Marquardt method [42] is used to regress for m_p and solved using Matlab (MathWorks, Inc. Natick, MA, USA) (Supplemental III). Statistical significance between m_p is determined through ANOVA (single factor) and the presented errors are the standard deviations. P-values less than 0.05 are accepted as indicating a statistical significant difference. Data are analyzed and plotted using Excel-2007 (Microsoft; Redmond, WA).

Determining plasma membrane permeability, m_{plm}

The rate of H_2O_2 uptake for each cell line is measured in the same manner as described by Wagner et al. [43] and used in Section 3.7. This assay provides an extracellular H_2O_2 removal rate, on a per cell basis. Briefly, $1.5\ x\ 10^4$ cells are seeded in 96-well culture (Corning, Union City, CA, USA) treated dishes and incubated 48 h prior to the assay at 37˚C, 5% CO_2; 90% confluency is reached. An extracellular bolus of 20 µM H_2O_2 (Sigma-Aldrich, St. Louis, MO, USA) is introduced in 5 min intervals to defined wells containing cells. The quenching solution described in Section 3.7 is used to terminate the assay. The fluorescent signal is detected using the same method described in Section 3.7. Wells containing cells were trypsinized and the number of cells were determined using a Moxi Z Mini Automated Cell Counter.

The transient data for C_{ext} is used to determine the value of the plasma membrane permeability, m_{plm}, by regression using the complete model,

$$V_{ext}\frac{dC_{ext}}{dt} = M_{in}\delta(t) - m_{plm} A_{cell} n_{cell}\left(\varphi_{plm} C_{ext} - C_{in}\right) \tag{4}$$

$$V_{in}\frac{dC_{in}}{dt} = m_{plm} A_{cell}\left(\varphi_{plm} C_{ext} - C_{in}\right) - m_p A_p n_p\left(\varphi_p C_{in} - C_p\right) \tag{5}$$

$$V_p\frac{dC_p}{dt} = m_p A_p\left(\varphi_p C_{in} - C_p\right) - k_2 C_{cat_p} C_p V_p. \tag{6}$$

where all parameters except m_{plm} are known. The Levenberg-Marquardt method discussed in Section 3.7 is used for regression (Supplemental IV). Statistical analysis of m_{plm} is determined through ANOVA (single factor) and the errors are presented as the standard deviations. Cells are counted at the end of the experiment. P-values less than 0.05 are accepted as indicating a statistical significant difference. Data are analyzed and plotted using Excel-2007 (Microsoft; Redmond, WA), and SigmaPlot (Systat Software Inc; San Jose, CA, USA) software.

Clonogenic assessment

Glioblastoma cells (2.5×10^4) are seeded in 6-well culture (Corning, Union City, CA, USA) treated dishes and exposed to appropriate H_2O_2 doses 48 h later. The external volume, V_{ext}, for the clonogenic plates is $2.5\ x\ 10^3$ μL. H_2O_2 exposures of (0 - 90 μM) are diluted in the appropriate culture media and cells are exposed for 1 h at 37°C. This dosing range is constituent with the extracellular H_2O_2 related to extracellular ascorbate dosing [44]. After exposure, the diluted media is removed, cells are trypsinized and counted with the Moxi Z Mini Automated Cell Counter and re-plated at 100 cells mL^{-1} in triplicates with appropriate media in 6-well culture treated dishes. Plates are incubated for two weeks at 37°C, 5% CO_2 and colonies form between 10 to 14 d at 37°C. Following a two-week incubation period, the colonies are fixed with 70% ethanol and stained with Coomasie Brilliant Blue R-250 (1610436; BioRad, Hercules, CA). Colonies with more than 50 cells are counted using a Counter-Pen (3133; Traceable Products, Webster, TX). The plating efficiency (PE) and surviving fraction (SF) are determined; PE = (colonies counted/cells plated) x 100 and SF = (PE of treated sample/PE of control) x 100 [45,46].

The average external H_2O_2 concentration ($\overline{C}_{ext}$) for each study was determined by directly using the Eqns (4)- (6), the external volume during the clonogenic assay, and the cell-specific parameters (Table 1) to first determine $C_{ext}(t)$ during dosing. $\overline{C}_{ext}$ for each experimental case and cell type was determined using Eqn (21). Statistical significance between each H_2O_2 exposure dose and cell types or cell modification is determined through ANOVA (Single Factor). P-values less than 0.05 are accepted as indicating a statistical significant difference. Data are analyzed and plotted using Excel-2007 (Microsoft; Redmond, WA). Error bars represent the standard error (SE). Clonogenic results for pancreatic cells were determined previously [30] and average concentrations for dosing are adjusted as described here.

Results and Discussion

Parameters for determining θ_{ss}

Table 1 summarizes the parameters used for each of the cell lines to determine the dimensionless intracellular H_2O_2 concentration, θ_{ss}. Overall, cell physical properties are similar however, there is a substantial range in the peroxisome catalase concentration and plasma membrane permeability across cell lines. The peroxisome catalase concentration ranges from $(7.98 \pm 5.69)\ x\ 10^{-6}\ M$ (MIA PaCa-2) to $(10.8 \pm 6.3)\ x\ 10^{-5} M$ (U-87). Across cell lines, the plasma membrane permeability ranged from $(2.23 \pm 1.72)\ x\ 10^{-6}\ m\ s^{-1}$ (siAQP3 MIA PaCa-2) to $(7.14 \pm 2.72)\ x\ 10^{-6}\ m\ s^{-1}$ (MIA PaCa-2). The peroxisome membrane permeability showed less variability across cell lines, however the value for H6c7 ($(0.38 \pm 0.17)\ x\ 10^{-5}\ m\ s^{-1}$) deviates significantly from the remaining cell lines analyzed which have an average of $(1.87 \pm 0.24)\ x\ 10^{-5}\ m\ s^{-1}$. The combined variability of the above parameters, as well as others could significantly alter θ_{ss}.

Table 1: Summary of Cellular Parameters by Cell Type

Variable	Variable (Units)	MIA PaCa-2	MIA PaCa-2 SiAQP3	H6c7 Cells	Reference/Notes
Cell Radius	(m)	$(8.29 \pm 1.13)\ x\ 10^{-6}$	$(8.29 \pm 1.13)\ x\ 10^{-6}$	$(8.74 \pm 0.14)\ x\ 10^{-6}$	Moxi[Z] N = 3
Cell Area	$A_{cell}\ (m^2)$	$(0.87 \pm 0.27)\ x\ 10^{-9}$	$(0.87 \pm 0.27)\ x\ 10^{-9}$	$(0.97\ \pm 0.03)\ x\ 10^{-9}$	Calculated
Cell Volume	$V_{cell}(m^3)$	$(2.52 \pm 0.98)\ x\ 10^{-15}$	$(2.52 \pm 0.98)\ x\ 10^{-15}$	$(\ 2.8 \pm 0.13)\ x\ 10^{-15}$	Moxi[Z] N = 3
Nucleus Volume	(m^3)	$(1.67 \pm 0.15)\ x\ 10^{-15}$	$(1.67 \pm 0.15)\ x\ 10^{-15}$	$(1.43 \pm 0.16)\ x\ 10^{-15}$	Dapi Confocal N = 4/5
Cell Volume without Cell Nucleus	(m^3)	$8.5\ x\ 10^{-16}$	$8.5\ x\ 10^{-16}$	$1.4\ x\ 10^{-15}$	Calculated
Plasma Membrane Partitioning Coefficient	φ_{plm}	1	1	1	Assumption
Number peroxisomes	n_p	$(310\ \pm 115\ )$	$(310\ \pm 115\ )$	$(374 \pm\ 117)$	GFP Confocal N = 6
Peroxisome Volume	$V_p(m^3)$	$(8.59\ \pm 4.85)\ x\ 10^{-20}$	$(8.59\ \pm 4.85)\ x\ 10^{-20}$	$(1.87 \pm 1.59)\ x\ 10^{-19}$	Spherical Estimation GFP Confocal N = 6
Peroxisome Area	$A_p(m^2)$	$(9.12\ \pm 3.41)x\ 10^{-13}$	$(9.12\ \pm 3.41)x\ 10^{-13}$	$(1.49 \pm 0.81)\ x\ 10^{-12}$	GFP Confocal N = 6
Active Catalase Monomers	--	(128,000 $\pm$ 37,200)	(128,000 $\pm$ 37,200)	(399,000 $\pm$ 23,900)	Catalase free in solution studies
Catalase Concentration in Peroxisome	$[C_{cat}]_p(M)$	$(\ 7.98\ \pm\ 5.69)\ x\ 10^{-6}$	$(\ 7.98\ \pm\ 5.69)\ x\ 10^{-6}$	$(\ 9.48\ \pm\ 8.61)\ x\ 10^{-6}$	Propagated error
Catalase Rate per peroxisome	$k_p(s^{-1})$	136	136	161	Calculated
Catalase Concentration in Cell	$[C_{cat}]_{cell}\ (mol\ m^3)$	$(8.45\ \pm\ 4.11)\ x\ 10^{-8}$	$(8.45\ \pm\ 4.11)\ x\ 10^{-8}$	$(2.37\ \pm\ 0.18)\ x\ 10^{-7}$	Propagated error
Catalase Rate Constant per Monomer	k_{chance} $(M^{-1}\ s^{-1})$	$1.7\ x\ 10^{7}$	$1.7\ x\ 10^{7}$	$1.7\ x\ 10^{7}$	[37]
Plasma Membrane Permeability	m_{plm} $(m\ s^{-1})$	$(7.14 \pm 2.72)\ x\ 10^{-6}$	$(2.23 \pm 1.72)\ x\ 10^{-6}$	$(2.56 \pm 0.79)\ x\ 10^{-6}$	Regressed
Peroxisome Membrane Permeability	m_p $(m\ s^{-1})$	$(2.13 \pm 1.21)\ x\ 10^{-5}$	$(2.13 \pm 1.21)\ x\ 10^{-5}$	$(0.38 \pm 0.17)\ x\ 10^{-5}$	Regressed
Peroxisome Membrane Partition Coefficient	φ_p	1	1	1	Assumption

Variable	Variable (Units)	U-87	T98G	LN-229	Reference/Notes
Cell Radius	(m)	$(9.49 \pm 0.20)\ x\ 10^{-6}$	$(10.1 \pm 0.50)\ x\ 10^{-6}$	$(8.22 \pm 1.37)\ x\ 10^{-6}$	Moxi[Z] N = 3
Cell Area	$A_{cell}\ (m^2)$	$(1.13 \pm 0.05)\ x\ 10^{-9}$	$(1.29 \pm 0.12)\ x\ 10^{-9}$	$(8.79 \pm 2.35)\ x\ 10^{-10}$	Calculated
Cell Volume	$V_{cell}(m^3)$	$(3.58 \pm 0.23)\ x\ 10^{-15}$	$(4.36 \pm 0.64)\ x\ 10^{-15}$	$(2.52 \pm 1.17)\ x\ 10^{-15}$	Moxi[Z] N = 3
Nucleus Volume	(m^3)	$(1.43 \pm 0.26)\ x\ 10^{-15}$	$(1.79 \pm 0.28)\ x\ 10^{-15}$	$(2.34 \pm 0.11)\ x\ 10^{-15}$	Dapi Confocal N = 3
Cell Volume without Cell Nucleus	(m^3)	$2.2\ x\ 10^{-15}$	$2.6\ x\ 10^{-15}$	$1.8\ x\ 10^{-16}$	Calculated
Plasma Membrane Partitioning Coefficient	φ_{plm}	1	1	1	Assumption
Number peroxisomes	n_p	$(211\ \pm 24)$	$(231\ \pm 74)$	$(296\ \pm 77)$	GFP Confocal N = 4
Peroxisome Volume	$V_p(m^3)$	$(6.4 \pm 3.5)\ x\ 10^{-20}$	$(9.2 \pm 5.6)\ x\ 10^{-20}$	$(5.8 \pm 1.2)\ x\ 10^{-20}$	Spherical Estimation GFP Confocal N = 4
Peroxisome Area	$A_p(m^2)$	$(9.4 \pm 4.1)\ x\ 10^{-13}$	$(1.5 \pm 0.82)\ x\ 10^{-12}$	$(8.1 \pm 4.0)\ x\ 10^{-13}$	GFP Confocal N = 4
Active Catalase Monomers	--	$(875{,}000 \pm 152{,}000)$	$(794{,}000 \pm 51{,}000)$	$(439{,}000 \pm 48{,}000)$	Catalase free in solution studies
Catalase Concentration in Peroxisome	$[C_{cat}]_p(M)$	$(1.08 \pm\ 0.63)\ x\ 10^{-4}$	$(6.21 \pm 4.29)\ x\ 10^{-5}$	$(4.25 \pm\ 1.49)\ x\ 10^{-5}$	Propagated error
Catalase Rate per Peroxisome	$k_p(s^{-1})$	$1.83\ x\ 10^3$	$1.05\ x\ 10^3$	$7.22\ x\ 10^2$	Calculated
Catalase Concentration in Cell	$[C_{cat}]_{cell}\ (mol\ m^3)$	$(4.06 \pm\ 0.75)\ x\ 10^{-7}$	$(3.02\ \pm\ 0.49)\ x\ 10^{-7}$	$(2.89 \pm\ 1.38)\ x\ 10^{-7}$	Propagated error
Catalase Rate Constant per Monomer	k_{chance} $(M^{-1}\ s^{-1})$	$1.7\ x\ 10^7$	$1.7\ x\ 10^7$	$1.7\ x\ 10^7$	[37]
Plasma Membrane Permeability	m_{plm} $(m\ s^{-1})$	$(2.52 \pm 1.02)\ x\ 10^{-6}$ (N = 3)	$(5.70 \pm 1.53)\ x\ 10^{-6}$ (N = 3)	$(3.03 \pm 0.67)\ x\ 10^{-6}$ (N = 4)	Regressed for N = 3/3/4
Peroxisome Membrane Permeability	m_p $(m\ s^{-1})$	$(1.55 \pm 0.79)\ x\ 10^{-5}$ (N = 4)	$(1.87 \pm 1.22)\ x\ 10^{-5}$ (N = 3)	$(1.94 \pm 0.87)\ x\ 10^{-5}$ (N = 3)	Regressed for N =4/3/3
Peroxisome Membrane Partition Coefficient	φ_p	1	1	1	Assumption

θ_{ss} and its validation of lumped parameter assumption

As mentioned above in Section 2.4, the θ_{ss} approximation is appropriate provided $\theta_{\eta=0}/\theta_{\eta=1} \sim 1$ (Eqn (19)). Using this approach, all cell lines show reasonable spatial independence. Table 2 summarizes the results for the cell lines used in this study. Graphical results for these cases are illustrated in Supplemental V.

We calculated θ_{ss} for each cell line using Eqn (7) and the specific properties listed in Table 1 for each cell line investigated. Error in θ_{ss} is determined by propagating error from the related parameters. Table 2 provides the calculated θ_{ss} for each cell line.

Table 2: θ_{ss} and Parameters Used to Verify Spatial Independence

	Cell Type	Bi_c	ϕ_c	$\theta_{\eta=0}/\theta_{\eta=1}$	θ_{ss}
Pancreatic Cells	MIA PaCa-2 Unmodified	0.04	0.360	0.98	0.73 ± 0.17
	MIA PaCa-2 siAQP3	0.01	0.360	0.98	0.45 ± 0.28
	H6c7	0.02	0.572	0.95	0.58 ± 0.19
Glioblastoma Cells	U-87	0.02	0.271	0.99	0.51 ± 0.18
	T98G	0.04	0.364	0.98	0.59 ± 0.20
	LN229	0.02	0.948	0.86	0.44 ± 0.16

Sensitivity of internal H_2O_2 to each parameter (membrane permeability and catalase activity)

The normalized local sensitivity analysis for each cell line is presented in Table 3 for various initial conditions for the three parameters m_{plm}, C_{cat_p}, and m_p. Supplemental VI provides a more complete listing for these and other variables.

It can be seen that, for the initial conditions used, θ_{ss} is typically more sensitive to relative changes in the plasma membrane and peroxisome permeabilities than changes in catalase concentrations. This may imply that the plasma membrane permeability could potentially be a target if intracellular H_2O_2 concentration is found to be effective for specific cell types.

Table 3: Normalized Local Sensitivity of θ_{ss} wrt m_{plm}, C_{cat_p}, and m_p

Cell Type	$s_{\theta_{ss},m_{plm}}$	$s_{\theta_{ss},C_{cat_p}}$	s_{θ_{ss},m_p}
MIA PaCa-2 Unmodified	0.20	-0.12	-0.07
MIA PaCa-2 siAQP3	0.25	-0.16	-0.09
H6c7	0.24	-0.04	-0.21
U-87	0.25	-0.03	-0.22
T98G	0.24	-0.05	-0.19
LN-229	0.25	-0.07	-0.18

Plasma Membrane Peroxiporins are Potential Drug Targets for Improving Ascorbate Therapy

Recently, we qualitatively showed that the expression of the peroxiporins, AQP3, was a significant factor in the susceptibility of the pancreatic cancer cell line, MIA PaCa-2 when exposed to extracellular H_2O_2, *in-vitro* [30]. This work was done by silencing AQP3 which reduced its expression by 90%. This corresponded to a 2.5 increase in cell survivability in the clonogenic assay. In the current study, we show that the corresponding membrane permeability of the MIA PaCa-2 cells reduced from $(7.14 \pm 2.72)\ x\ 10^{-6}\ m\ s^{-1}$ to $(2.23 \pm 1.72)\ x\ 10^{-6}\ m\ s^{-1}$ when AQP3 was reduced by 90%. Thus, the

peroxiporin AQP3 accounts for nearly 80% of the permeability of H_2O_2 in MIA PaCa-2. From our mathematical analysis, the silencing of AQP3 for MIA PaCa-2 corresponds to a change in θ_{ss} from 0.73 ± 0.17 to 0.45 ± 0.28 which is not statistically significant (p = 0.21). However, the significant change in cell survivability results from our previous study suggests that this difference may be significant with reduced error in the estimated parameters.

These results imply that, when ascorbate therapy is sensitive to the intracellular H_2O_2 concentration, the plasma membrane permeability, via peroxiporins, may be a viable drug target for additional enhancement of ascorbate therapy. The sensitivity analysis of how much the intracellular H_2O_2 concentration may change with plasma membrane permeability can provide insight to the potential success in targeting peroxiporins (Figure 5).

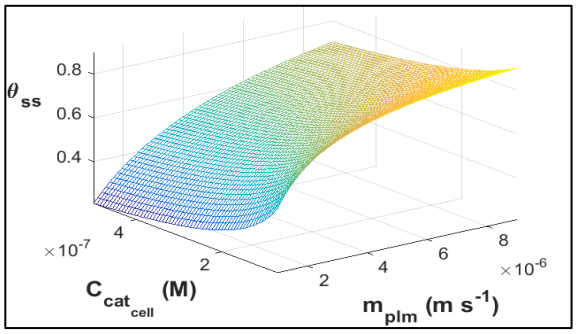

Figure 5. Sensitivity of the steady-state ratio of intracellular to extracellular H_2O_2, θ_{ss}, for catalase concentration, C_{cat_p}, and plasma membrane permeability, m_{plm}. All other parameters are based on values obtained for MIA PaCa-2. As can be seen, for this case, increasing m_{plm} increases θ_{ss} but the rate of increase decreases at higher plasma membrane permeabilities. The sensitivity analysis is useful for other susceptible cancer cell lines in determining whether elements related to m_{plm}, such as peroxiporin expression, may benefit from drug targeting.

As mentioned in the Introduction (Section 1.), the nucleoside analog gemcitabine can increase AQP3 by a factor of eight in some cancer cells [34]. For the susceptible cancer cell line MIA PaCa-2, this would increase the value for θ_{ss} during dosing by a factor of 1.3. This could be very significant when near maximum dosing.

No relationship between intracellular H_2O_2 concentration and ascorbate susceptibility

One can immediately see from Table 2 that there is little variation within the error in θ_{ss} across the cell types investigated in this study. If intracellular H_2O_2 concentration provides a unique relationship to susceptibility, then a correlation should exist between the calculated θ_{ss} for each cell type and their susceptibility to ascorbate dosing [5]. However, as shown in Figure 6, there is no significant difference between the calculated θ_{ss} and the reported EC_{50} ascorbate susceptibility for each cell line [1,5,6]. Thus, there is no unique relationship between θ_{ss} and ascorbate susceptibility for ascorbate dosing. As error in θ_{ss} is due to the propagation of error in the associated parameters, improved methods for determining said parameters may result in a significant difference in values. However, these corrections are not likely to significantly improve the relative range in θ_{ss} across the susceptibility scale for cell types. This is most pronounced when comparing θ_{ss} for the normal pancreatic cell line, H6c7, which is unaffected by ascorbate dosing, with θ_{ss} for the highly susceptible pancreatic cancer cell line, MIA PaCa-2 (p = 0.36). Since MIA PaCa-2 is responsive at ascorbate dosing values that are over an order-of-magnitude less than the dosing used for the non-responsive H6c7, other factors are likely responsible for the cellular response for these two cell lines.

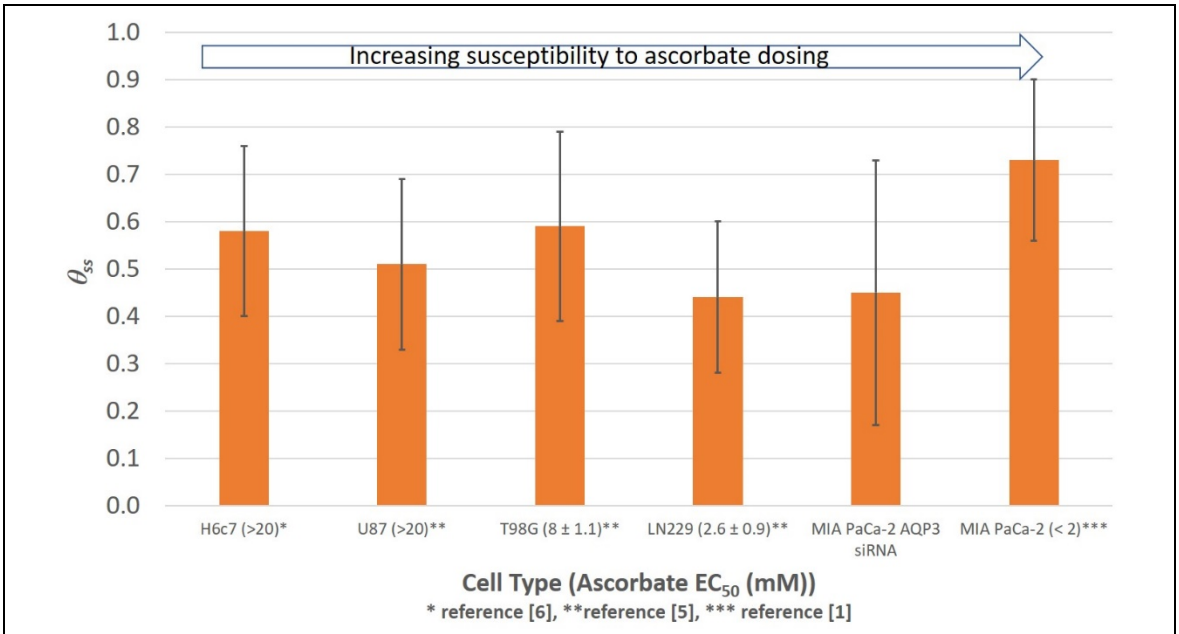

Figure 6. Ascorbate dosing does not correlate with intracellular H_2O_2 concentration. There appears to be no general trend between calculated θ_{ss} and the EC_{50} for ascorbate dosing for the cell types examined [1,5,6]. If the proposed hypothesis is correct, the effective intracellular H_2O_2 concentration would be unique in determining susceptibility across cell lines, and the calculated θ_{ss} would increase with increased susceptible.

Clonogenic response vs. initial extracellular H_2O_2 concentration for glioblastoma cell lines

The clonogenic assay of MIA PaCa-2 for dosing with extracellular H_2O_2 up to 90 µM has been previously shown [30]. Figure 7 shows the clonogenic response to extracellular H_2O_2 dosing as normalized surviving fraction for the three glioblastoma cell lines studied, LN-229, T98G, and U-87. Recall that LN-229 was found to be sensitive to ascorbate dosing while T98G was found to be only moderately sensitive and U-87 was found to be insensitive [5]. As can be seen, only LN-229 cell line shows a significant dosing response for extracellular H_2O_2 dosing up to 90 µM. These results are consistent with the ascorbate dosing, although the T98G cell line shows no significant response to the H_2O_2 dosing in this study.

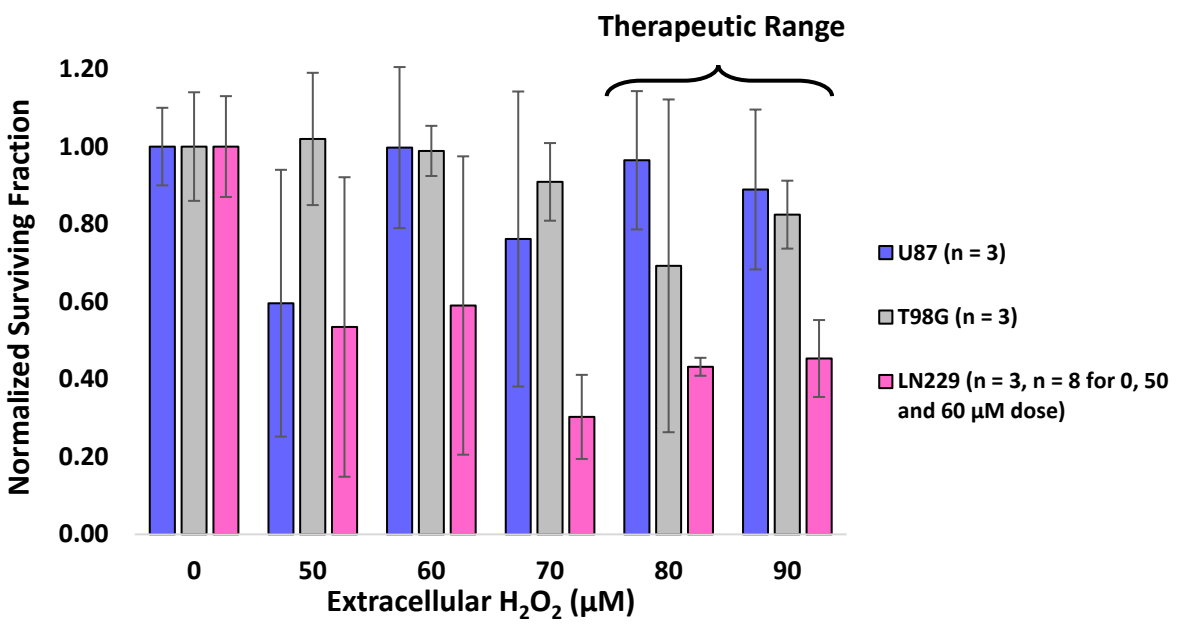

Figure 7. Dose response of glioblastoma cell lines for exposure of bolus H_2O_2 concentrations. Surviving fraction, relative to 0 µM H_2O_2, for U-87 and T98G cells are not significantly affected for dosing range evaluated. Surviving fraction, relative to 0 µM H_2O_2 is significantly decreased for LN-229 therapeutic dosing of initial H_2O_2 exposure at 80 µM and 90 µM. Error bars displayed represent the standard error (SE).

The relationship between intracellular H_2O_2 concentration and H_2O_2 clonogenic response is not unique

We investigate whether a direct correlation exists between extracellular H_2O_2 concentration clonogenic response and the intracellular concentration. First, we recognize that the extracellular H_2O_2 concentration can reduce during the clonogenic studies due to its uptake by the cells. Thus, we use the average external dosing concentration ($\overline{C}_{ext}$) calculated using Eqn (21). Using the definition of θ_{ss} with ($\overline{C}_{ext}$), we determine the average intracellular H_2O_2 concentration during extracellular H_2O_2 dosing. Figure 8 shows these results for each of the cell lines investigated in this work. The error in C_{in} is the standard deviation representing the range in intracellular H_2O_2 concentration based from the calculated θ_{ss} for each dose exposure. The error in the clonogenic response (surviving fraction) represent the standard error (SE). The data used in Figure 8 can be found in Supplement VII.

It is immediately apparent from Figure 8 that the clonogenic surviving fraction does not correspond to a unique function of intracellular H_2O_2 concentration. Furthermore, non-responsive cell lines have significantly higher surviving fractions for the same calculated intracellular H_2O_2 concentration.

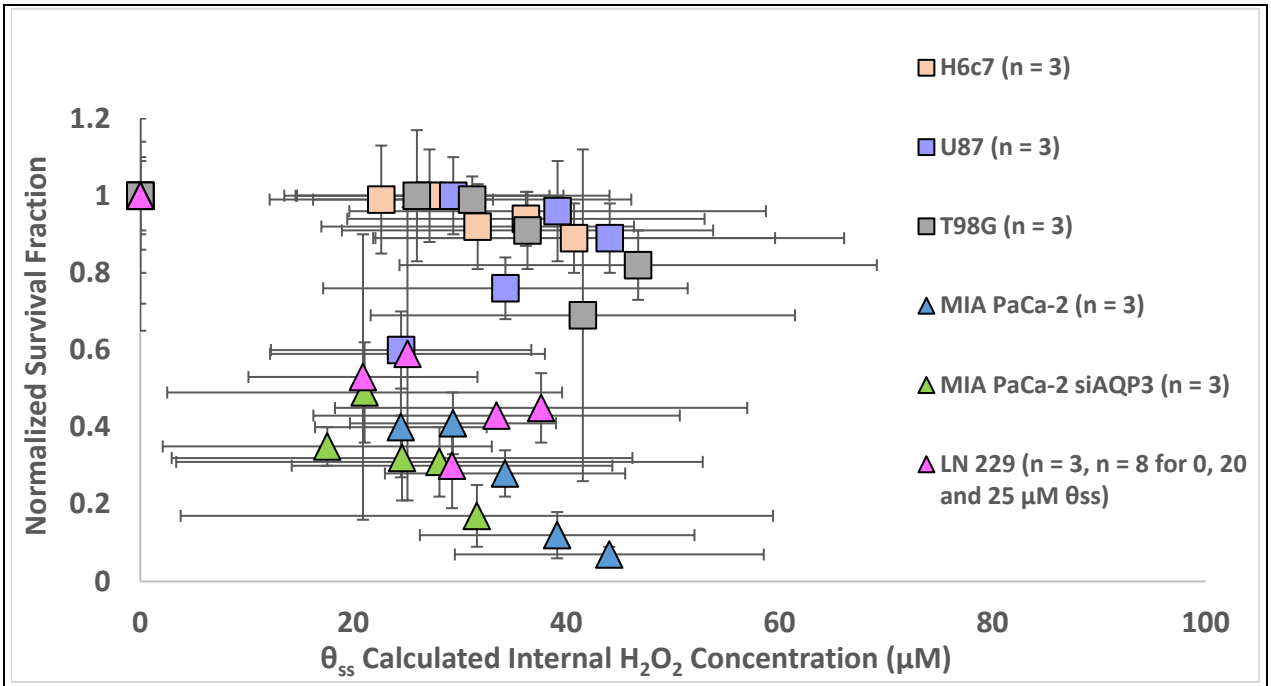

Figure 8. Elevated intracellular H_2O_2 concentrations does not necessarily decrease the surviving fraction of cells. The normal and H_2O_2 non-responding cells (squares) have equally high intracellular H_2O_2 concentrations as compared to the H_2O_2-susceptible cells (triangles). These results indicate that the intracellular H_2O_2 concentration is handled differently and is cell-dependent. It can therefore be concluded that the clonogenic response relative to intracellular H_2O_2 concentration is cell type dependent. The vertical error bars represent the standard error from the clonogenic surviving fraction studies. The horizontal error bars represent the propagated error for the calculated intracellular H_2O_2 concentration range at the respective dose.

Results of this work implies a complex relationship between intracellular H_2O_2 and clonogenic response

It has been established that P-AscH$^-$ therapy is effective due to the associated high H_2O_2 flux into susceptible carcinoma cells with a significant labile iron pool (LIP) [i.e., 9,47]. The product of these two reactants, H_2O_2 and redox-active iron is the highly reactive hydroxyl radicals (·OH). When in the presence of unprotected DNA, ·OH can result in significant DNA damage [9].

Previous research found that an increased labile iron pool (LIP) in some cells resulted in an increase in the potential for oxidative stress [48,49]. Lipiński et al. (2000) found a factor of three increase in iron in the LIP for H_2O_2-sensitive lymphoma cells than that found in H_2O_2-resistant lymphoma cells [48]. However, Moser et al. (2014) investigated the LIP in pancreatic normal and tumor tissue (MIA PaCa-2) and found higher levels of labile iron in the normal tissue [50]. Thus, we hypothesized that the steady-state intracellular H_2O_2 concentration was the mitigating factor in determining susceptibility and that variations in the cell's transport and reaction parameters altered the available intracellular H_2O_2 for different cell types at similar dosing concentrations.

Results from this work clearly showed that the calculated intracellular H_2O_2, based on this catalase-dominant lumped-parameter model, is not unique with respect to cellular susceptibility for either extracellular exposure to ascorbate or H_2O_2 dosing. Nevertheless, Doskey et al. (2016) show that the ED_{50} results for clonogenic exposure to P-AscH$^-$ is directly coupled to the rate of H_2O_2 uptake per cell [51]. Further, we previously showed a significant dosing response for MIA PaCa-2 and siAQP3 MIA PaCa-2 for

extracellular H_2O_2 exposure [30]. Thus, the intracellular H_2O_2 concentration remains a significant factor in susceptibility, albeit the unifying mechanism that accounts for cell type dependency, is more complex than that which can be described by a linear correlation.

Many factors that vary with cell type and are not considered in this analysis might impact the unifying mechanism for cellular response to P-$AscH^-$ therapy. Examples include variations in localized chelators, impact on mitrochondrial redox processes, energy crisis and DNA protection [17,52]. Further, it is unclear in cancer mutations whether the non-catalase H_2O_2 enzymatic reactions such as glutathione peroxidases and peroxiredoxins remain negligible at pharmacological concentrations of H_2O_2. In addition, the relatively rapid flux of the hydroxyl radicals suggests that local spatial factors that vary with cell type, may also be significant.

Two important facts emerge from this research that can help in defining a unifying mechanism for cell susceptibility to ascorbate. First, relatively little variation in the dimensionless intracellular H_2O_2 concentration, when determined by a reaction diffusion model, is observed for susceptible and non-susceptible cells despite an order-of-magnitude difference in ascorbate dosing. Second, when cells are susceptible, their sensitivity to dosing is significant within a relatively narrow range. Thus, a unifying mechanism must account for these observations.

Conclusion

This work developed a mathematical model to determine the intracellular H_2O_2 concentration during extracellular H_2O_2 dosing equivalent to that expected during P-$AscH^-$ therapy. The model assumed that at high pharmacological concentrations of H_2O_2, catalase was the dominant mechanism for the removal of peroxide and other reactive enzymatic processes were not considered. Critical parameters such as membrane permeability were determined. The results demonstrate that there is not a unique intracellular H_2O_2 concentration that corresponds to a dosing response. These results suggest a more complex mechanism, which may include the other enzymatic reactions and spatial dependency, is necessary to captures cell type-dependency for susceptibility.

Acknowledgments

This research was funded by an endowment from Jacques S. Yeager, Sr. Special thanks go to Brett Wagner; Hong Xu, UCR Stem Cell Core; Andrea Cabrera; Soroush Ardekani; Kaustabh Ghosh, Bahman Anvari. In memory of Jacques S. Yeager, Sr. The reviewers comments were greatly appreciated.

References

1 Du J, Martin SM, Levine M, Wagner BA, Buettner GR, Wang SH, *et al*. Mechanisms of ascorbate-induced cytotoxicity in pancreatic cancer. Clin Cancer Res. 2010;16(2): 509-520.

2 Du J, Cieslak JA, Welsh JL, Sibenaller ZA, Allen BG, Wagner BA, *et al*. Pharmacological ascorbate radiosensitizes pancreatic cancer. Cancer Res. 2015;75(16): 3314-3326.

3 Welsh JL, Wagner BA, Van't Erve TJ, Zehr PS, Berg DJ, Halfdanarson TR, *et al*. Pharmacological ascorbate with gemcitabine for the control of metastatic and node-positive pancreatic cancer (PACMAN): results from a phase I clinical trial. Cancer Chemoth Pharm. 2013;71(3): 765-775.

4 Cieslak JA, J Cullen JJ. Treatment of pancreatic cancer with pharmacological ascorbate. Curr Pharm Biotechno. 2015;16(9); 759-770.

5 Chen Q, Espey MG, Sun AY, Pooput C, Kirk KL, Krishna MC, *et al*. Pharmacologic doses of ascorbate act as a prooxidant and decrease growth of aggressive tumor xenografts in mice. Proc Natl Acad Sci USA. 2008;105(32): 11105-11109.

6 Chen Q, Espey MG, Krishna MC, Mitchell JB, Corpe CP, Buettner GR, *et al*. Pharmacologic ascorbic acid concentrations selectively kill cancer cells: action as a pro-drug to deliver hydrogen peroxide to tissues. Proc Natl Acad Sci USA. 2005;102(32): 13604-13609.

7 Du J, Cullen JJ, Buettner GR. Ascorbic acid: chemistry, biology and the treatment of cancer. BBA-Rev Cancer. 2012;1826(2): 443-457.

8 Chen Q, Espey MG, Sun AY, Lee JH, Krishna MC, Shacter E, *et al*. Ascorbate in pharmacologic concentrations selectively generates ascorbate radical and hydrogen peroxide in extracellular fluid in vivo. Proc Natl Acad Sci USA. 2007;104(21): 8749-8754.

9 Schoenfeld et al., O_2.- and H_2O_2-Mediated Disruption of Fe Metabolism Causes the Differential Susceptibility of NSCLC and GBM Cancer Cells to Pharmacological Ascorbate, Cancer Cell (2017), http://dx.doi.org/10.1016/j.ccell.2017.02.018

10 Herst PM, Broadley KW, Harper JL, McConnell MJ. Pharmacological concentrations of ascorbate radiosensitize glioblastoma multiforme primary cells by increasing oxidative DNA damage and inhibiting G2/M arrest. Free Radic Biol Med. 2012;52(8): 1486–1493.

11 Castro ML, McConnell MJ, Herst PM. Radiosensitisation by pharmacological ascorbate in glioblastoma multiforme cells, human glial cells, and HUVECs depends on their antioxidant and DNA repair capabilities and is not cancer specific. Free Radic Biol Med. 2014;74: 200–209.

12 Haber F., Weiss J. Über die Katalyse des Hydroperoxydes (On the catalysis of hydroperoxide). Naturwissenschaften. 1932;20(51): 948–950.

13 Chen P, Yu J, Chalmers B, Drisko J, Yang J, Li B, *et al*. Pharmacological ascorbate induces cytotoxicity in prostate cancer cells through ATP depletion and induction of autophagy. Anticancer Drugs. 2012;23(4): 437–444.

14 Shatzer AN, Espey MG, Chavez M, Tu H, Levine M, Cohen JI. Ascorbic acid kills Epstein-Barr virus positive Burkitt lymphoma cells and Epstein-Barr virus transformed B-cells in vitro, but not in vivo. Leuk Lymphoma. 2013;54(5): 1069–1078.

15 Ma Y, Chapman J, Levine M, Polireddy K, Drisko J, Chen Q. High-dose parenteral ascorbate enhanced chemosensitivity of ovarian cancer and reduced toxicity of chemotherapy. Sci Transl Med. 2014;6(222): 222ra18.

16 Cieslak JA, Strother RK, Rawal M, Du J, Doskey CM, Schroeder SR, *et al*. Manganoporphyrins and ascorbate enhance gemcitabine cytotoxicity in pancreatic cancer. Free Radic Biol Med. 2015;83: 227–237.

17 Buranasudja V, Doskey CM, Wagner BA , Du J, Gordon DJ , Koppenhafer S, Cullen JJ, Buettner GR. 236-DNA Damage and Energy Crisis are Central in the Mechanism for the Cytotoxicity of Pharmacological Ascorbate in Cancer Treatment. Free Radic Biol Med. 2017;112(1):162.

18 Rawal M, Schroeder SR, Wagner BA, Cushing CM, Welsh J, Button AM, *et al*. Manganoporphyrins increase ascorbate-induced cytotoxicity by enhancing H_2O_2 generation**.** Cancer Res. 2013;73(16): 5232–5241.

19 Sestili P, Brandi G, Brambilla L, Cattabeni F, Cantoni O. Hydrogen peroxide mediates the killing of U937 tumor cells elicited by pharmacologically attainable concentrations of ascorbic acid: cell death prevention by extracellular catalase or catalase from cocultured erythrocytes or fibroblasts. J Pharm Exp Ther. 1996;277(3): 1719–1725.

20 Tian J, Peehl DM, Knox SJ. Metalloporphyrin synergizes with ascorbic acid to inhibit cancer cell growth through fenton chemistry. Cancer Biother Radiopharm. 2010;25(4): 439–448.

21 Espey MG, Chen P, Chalmers B, Drisko J, Sun AY, Levine M, *et al*. Pharmacologic ascorbate synergizes with gemcitabine in preclinical models of pancreatic cancer. Free Radic Biol Med. 2011;50(11): 1610–1619.

22 Ranzato E, Biffo S, Burlando B. Selective ascorbate toxicity in malignant *meso*thelioma: a redox Trojan mechanism. Am J Respir Cell Mol Biol. 2011;44(1): 108–117.

23 Klingelhoeffer C, Kämmerer U, Koospal M, Mühling B, Schneider M, Kapp M, *et al*. Natural resistance to ascorbic acid induced oxidative stress is mainly mediated by catalase activity in human cancer cells and catalase-silencing sensitizes to oxidative stress. BMC Complement Alter Med. 2012;12(1): 61.

24 Ohno S, Ohno Y, Suzuki N, Soma G, Inoue M. High-dose vitamin C (ascorbic acid) therapy in the treatment of patients with advanced cancer. Anticancer res 2009;29(3):809-815.

25 Cohen G, Hochstein P. Glutathione Peroxidase: The Primary Agent for the Elimination of Hydrogen Peroxide in Erythrocytes. Biochemistry 1963; 2(6): 1420-1428.

26 Makino N, Mochizuki Y, Bannai S, Sugita Y. Kinetics Studies on the Removal of Extracellular Hydrogen Peroxide by Cultured Fibroblasts. J Biol. Chem. 1994; 269(2): 1020-1025.

27 Makino N, Sasaki K, Hashida K, Sakakura Y. A metabolic model describing the H_2O_2 elimination by mammalian cells including H2O2 permeation through cytoplasmic and peroxisomal membranes: comparison with experimental data, Biochimica et Biophysica Acta 2004;1673: 149-159.

28 Ng CF, Schafer FQ, Buettner GR, Rodgers VGJ. The rate of cellular hydrogen peroxide removal shows dependency on GSH: mathematical insight into in vivo H_2O_2 and GPx concentrations. Free Radic Res 2007;41(11):1201-1211.

29 Benade L, Howard T, Burk D. Synergistic killing of Ehrlich ascites carcinoma cells by ascorbate and 3-amino-1, 2, 4,-triazole. Oncology 1969;23(1):33-43.

30 Erudaitius, D, Huang A, Kazmi S, Buettner GR, Rodgers VGJ. Peroxiporin Expression Is an Important Factor for Cancer Cell Susceptibility to Therapeutic H_2O_2: Implications for Pharmacological Ascorbate Therapy, PloS One 2017;12(1): e0170442.

31 Bienert GP, Schjoerring JK, Jahn TP. Membrane transport of hydrogen peroxide. Biochimica et Biophysica Acta (BBA)-Biomembranes 2006;1758(8):994-1003.

32 Miller, Evan W, Dickinson BC, Chang CJ. Aquaporin-3 mediates hydrogen peroxide uptake to regulate downstream intracellular signaling. Proceedings of the National Academy of Sciences 2010;107(36):15681-15686.

33 Verkman AS, Hara-Chikuma M. Papadopoulos MC. Aquaporins—new players in cancer biology. J. of Molecular Medicine 2008;86(5):523-529.

34 Tigueros-Motos L, Perez-Torras S, Casado FJ, Molina-Arcas M, Pastor-Anglada M. Aquaporin 3 (AQP3) Participates in the Cytotoxic Response to Nucleoside-Drived Drugs. BMC Cancer 2012;12:434.

35 Antunes F, Cadenas E. Estimation of H_2O_2 gradients across biomembranes. FEBS Lett 2000;475(2):121-126.

36 Lim JB, Huang BK, Deen WM, Sikes HD. Analysis of the lifetime and spatial localization of hydrogen peroxide generated in the cytosol using a reduced kinetic model, Free Radic Biol Med 2015;89: 47-53.

37 Chance B. The kinetics of the enzyme-substrate compound of peroxidase, J Biol Chem 1943;151(2):553-577.

38 Yue H, Brown M, Knowles J, Wang H, Broomhead DS, Kell DB. Insights into the behaviour of systems biology models from dynamic sensitivity and identifiability analysis: a case study of an NF-κB signalling pathway, Molecular BioSystems 2006;2:640-649.

39 van Stroe-Blezen SAM, Everaerts FM, Janssen LJJ, Tacken RA. Diffusion coefficients of oxygen, hydrogen peroxide and glucose in a hydrogel. Analytzca Chmuca Acta 1993;273 553-560.

40 Ouyang H, Mou LJ, Luk C, Liu N, Karaskova J, Squire J, et al. Immortal human pancreatic duct epithelial cell lines with near normal genotype and phenotype. Am J Pathol. 2000;157(5): 1623–1631. pmid:11073822.

41 Aebi H. Catalase in vitro. Method Enzymol. 1984;105: 121-126.

42 Gavin H. The Levenberg-Marquardt method for nonlinear least squares curve-fitting problems. 2011;www.duke.edu/~hpgavin/lm.pdf.

43 Wagner BA, Witmer JR, van't Erve TJ, Buettner GR. An assay for the rate of removal of extracellular hydrogen peroxide by cells. Redox Biol. 2013;1(5): 210–217.

44 Doskey CM, van`t Erve TJ, Wagner BA, Buettner GR. Moles of a Substance per Cell Is a Highly Informative Dosing Metric in Cell Culture. PloS One. 2015; 10(7): e0132572. doi: 10.1371/journal.pone. 0132572 PMID: 26172833.

45 Franken NAP, Rodermond HM, Stap J, Haveman J, Bree CV. Clonogenic assay of cells in vitro. Nat Protoc. 2006;1: 2315–2319. pmid:17406473.

46 Munshi A, Hobbs M, Meyn RE. Clonogenic cell survival assay. Chemosensitivity: Volume 1 In Vitro Assays. 2005: 21–28.

47 Brandt KE, Falls KC, Schoenfeld JD, Rodman SN et al. Augmentation of intracellular iron using iron sucrose enhances the toxicity of pharmacological ascorbate in colon cancer cells. Free Radical Bio Med. 2018;14: 82-87.

48 Lipiński P, Drapier JC, Oliveira L, Retmańska H, Sochanowicz B, Kruszewski M. Intracellular iron status as a hallmark of mammalian cell susceptibility to oxidative stress: a study of L5178Y mouse lymphoma cell lines differentially sensitive to H_2O_2. Blood 2000;95(9):2960-6.

49 Du J, Wagner BA, Buettner GR, Cullen JJ. Role of labile iron in the toxicity of pharmacological ascorbate. Free Radical Bio Med. 2015;84: 289-295.

50 Moser JC, Rawal M, Brett A. Wagner, Du J, Cullen JJ, Buettner GR. Pharmacological ascorbate and ionizing radiation (IR) increase labile iron in pancreatic cancer. Redox Biol. 2014; 2: 22–27.

51 Doskey CM, Buranasudja V, Wagner BA, Wilkes JG, Du J, Cullen JJ, and Buettner GR. Tumor cells have decreased ability to metabolize H_2O_2: Implications for pharmacological ascorbate in cancer therapy. Redox Biology. 2016; 10:274-284.

52 Verrax J, Calderon PB. Pharmacologic concentrations of ascorbate are achieved by parenteral administration and exhibit antitumoral effects. Free Radical Bio Med. 2009; 47:32–40.